

An investigation of planetary nebulae accompanying PG 1159 central stars, based on Gaia DR2 measurements

Alaa Ali¹ and Wedad R. Alharbi²

¹ Department of Astronomy, Faculty of Science, Cairo University, 12613 Giza, Egypt; afouad@sci.cu.edu.eg

² Department of Physics, College of Science, University of Jeddah, 23890 Jeddah, Saudi Arabia; wralharbi@uj.edu.sa

Received 2020 November 12; accepted 2021 January 27

Abstract This article discusses the physical and kinematical characteristics of planetary nebulae accompanying PG 1159 central stars. The study is based on the parallax and proper motion measurements recently offered by the Gaia space mission. Two approaches were used to investigate the kinematical properties of the sample. The results revealed that most of the studied nebulae arise from progenitor stars in the mass range $0.9 - 1.75 M_{\odot}$. Furthermore, they tend to live within the Galactic thick disk and move with an average peculiar velocity of $61.7 \pm 19.2 \text{ km s}^{-1}$ at a mean vertical height of $469 \pm 79 \text{ pc}$. The locations of the PG 1159 stars on the H-R diagram indicate that they have an average final stellar mass and evolutionary age of $0.58 \pm 0.08 M_{\odot}$ and $25.5 \pm 5.3 \times 10^3 \text{ yr}$, respectively. We found a good agreement between the mean evolutionary age of the PG 1159 stars and the mean dynamical age of their companion planetary nebulae ($28.0 \pm 6.4 \times 10^3 \text{ yr}$).

Key words: planetary nebulae: general — methods: kinematics — stars: individual (PG 1159)

1 INTRODUCTION

Gaia¹ is a space mission launched and operated by the European Space Agency (ESA) to provide a precise three-dimensional map of our home galaxy (the Milky Way). Data were released in two versions; the first was Gaia Data Release 1 (DR1) in 2016 and the second was Gaia Data Release 2 (DR2) in 2018. Gaia provided astrometric and photometric data for about 1.7 billion sources, such as proper motion (μ), parallax (ϖ) and magnitude in three photometric filters; G, G_{BP} , G_{RP} (Brown et al. 2018). The parallax measurements from Gaia DR2 and the forthcoming Gaia data release (Gaia DR3) represent a substantial step in the way of solving the chronic problem of finding reliable distances for Galactic planetary nebulae (PNe).

Determining most, if not all, nebular parameters relies on their distances. It is known that only a few PNe have trusted distances that are determined by one of these individual methods; trigonometric parallax, spectroscopic parallax, cluster membership and angular expansion. There are other less reliable statistical methods applied to determine PN distances, such as the relationships between

the nebular ionized mass and both its optical depth and its radius. For more discussion on these methods, see Ali et al. (2015) and Frew et al. (2016) and references therein. Although trigonometric parallax is one of the most reliable and direct methods for measuring PN distances, it has been applied to only a few PNe (e.g. Harris et al. 2007; Acker et al. 1998; Pottasch & Acker 1998) before the Gaia era. Distances for most stars in Gaia DR2 could not be calculated directly from their parallax angles since these angles were measured utilizing a complicated iterative technique that includes different assumptions. Bailer-Jones et al. (2018) applied a correct inference procedure to represent the nonlinearity of the transformation and asymmetry of the resulting probability distribution. The uncertainty in the distance assessment is represented by the lower and upper limits of the asymmetric confidence interval. Therefore, in this study, we adopt the distances taken from Bailer-Jones et al. (2018).

All stars born with initial masses $\leq 8.0 M_{\odot}$ will end their lives as white dwarfs (WDs). The evolution of the star between the asymptotic giant branch (AGB) and the WD phase takes a short time compared to the preceding evolutionary phases. During this short transition, all stars that start their evolution with hydrogen and

¹ More details regarding the Gaia mission are available at <http://sci.esa.int/gaia/>

helium burning shells (post-AGB) will end their lives with carbon-oxygen WD cores (Werner & Herwig 2006). The central stars (CSs) of PNe can be divided into two main groups according to the hydrogen abundance in their atmospheres (Mendez 1991). The first group “hydrogen-rich” has relative hydrogen abundance close to the cosmic value, while the second group “hydrogen-deficient” has high abundances of helium and carbon with a tiny (or free) amount of hydrogen. The stellar spectra of the latter group are dominated by broad and intense emission lines typical of Wolf-Rayet [WR] stars, frequently of [WC] subtype and sometimes of [WO]. The spectra of some hydrogen-deficient stars reveal the presence of helium, carbon and oxygen absorption lines. This class was named PG 1159 after the detection of its prototype star PG 1159–035. In addition, there is a small set of stars that has the same properties of PG 1159 class but their spectra show some hydrogen absorption lines that are named hybrids-PG 1159 (Napiwotzki & Schoenberner 1991). The PG 1159 stellar class is characterized by effective temperature (T_{eff}) ranging from 7500 K to 25000 K and logarithmic surface gravity ($\log g$) from 5.5 cm s^{-2} to 8.0 cm s^{-2} (Löbbling et al. 2019). Werner & Herwig (2006) reported an evolutionary sequence for hydrogen-deficient C-rich stars as follows: AGB \rightarrow [WC] \rightarrow PG 1159 \rightarrow DO.

The main objective of the present work is to determine the kinematical and physical parameters of PNe accompanying PG 1159 CSs. The rest of the article is structured as follows. Section 2 presents the data sample. Sections 3 and 4 inspect the physical and kinematical properties of the selected sample, respectively. Section 5 discusses the status of the four nebulae A 21, IeWe 1, Sh 2-78 and NGC 650, while we draw our conclusions in Section 6.

2 THE SAMPLE

An update of the CS catalog of Weidmann & Gamen (2011) has been recently published by Weidmann et al. (2020). The new catalog contains the spectral classification of 620 CSs of confirmed and probable PNe compared with 492 in the old catalog. Examining the new catalog and other literature, we obtained an initial sample of 22 PNe accompanying PG 1159 CSs (PNe-PG 1159). The CSs of A 43, NGC 7094 and Sh 2-68 have spectral characteristics of hybrids-PG 1159. The CSs of A 30, A 78 and NGC 2371–72 are classified as stars in the transition phase between WC and PG 1159. The spectrum of WC-PG 1159 class shows properties of both WC and PG 1159 stars. These three nebulae were excluded from our sample, and hence our final sample consists of 19 PNe-PG 1159. Table 1 summarizes the basic data of the PNe-PG 1159 sample. It lists the PN name, galactic (L , B) and equatorial

(α , δ) coordinates, angular radius (θ), line of sight velocity (V_{los}), expansion velocity (V_{exp}), Gaia DR2 designation, distance (D), proper motion (PM_{α} , PM_{δ}), G-magnitude (m_G) and color index ($BP - RP$). The PN coordinates and angular radii were collected from the SIMBAD database and table 10 in Frew et al. (2016), respectively, while the PN radial and expansion velocities are from Acker et al. (1992) and Frew et al. (2016). The CS parameters are compiled from the Gaia DR2 catalog. It should be noted that the CS is the source of ultraviolet (UV) radiation that ionizes the gas within the nebular shell, and hence it appears as a blue star. The measurements of $BP - RP$ listed in Table 1 affirm that all PG 1159 stars are blue stars except Sh 2–68 is red. The reason behind the observed red color of Sh 2–68 may be attributed to either the high reddening along its line of sight direction or to visible light being dominated by its close main sequence binary companion.

To investigate the kinematical properties of PNe-PG 1159, we followed two approaches. The first is to build the $\sqrt{U_{\text{LSR}}^2 + W_{\text{LSR}}^2} - V_{\text{LSR}}$ “Toomre diagram,” while the second is to calculate the peculiar velocity of the sample.

3 PHYSICAL CHARACTERISTICS OF THE SAMPLE

It is noticeable from Table 1 that about half the sample objects are located at high galactic latitudes with a mean absolute value of 20.5° . Moreover, the determined mean vertical height (Z) is $469 \pm 79 \text{ pc}$ (Table 4). The latter result indicates that most PNe-PG 1159 reside inside the Galactic thick disk, which has a mean vertical height of $510 \pm 40 \text{ pc}$ (Carollo et al. 2010), and hence they are frequently members of Galactic population II. In Table 2, we present the PN radius calculated from its angular radius and distance. The dynamical (kinematical) age of the PN was calculated from its derived radius and expansion velocity. The analysis of these two parameters indicated that this class of PNe has large sizes and long ages. Throughout the PN evolution, its size and mass increase while its density decreases. The results reported in Table 2 show an average radius of $0.60 \pm 0.13 \text{ pc}$, which is approximately six times the standard PN radius (0.1 pc ; Pottasch 1983) and an average dynamical age of $28.0 \pm 6.4 \times 10^3 \text{ yr}$, which is nearly three times the standard value ($10.0 \times 10^3 \text{ yr}$; Pottasch 1983). The expansion velocity of a PN is not constant but it varies during the nebular evolution as a result of variation of the stellar wind parameters throughout PN dynamical evolution. Therefore, we should regard the dynamical age with caution when discussing the physical parameters of PNe.

Table 3 lists the effective temperature, surface gravity and luminosity of the PG 1159 CSs. The effective

Table 1 Basic Data on the PNe-PG 1159 Sample

PN designation	PN parameters										CS parameters				
	$L(^{\circ})$	$B(^{\circ})$	α	δ	$\theta(^{\prime\prime})$	$V_{\text{los}} (\text{km s}^{-1})$	$V_{\text{exp}} (\text{km s}^{-1})$	Gaia DR2 ID	D (pc)	$PM_{\alpha} (\text{mas yr}^{-1})$	$PM_{\delta} (\text{mas yr}^{-1})$	m_G	$BP - RP$		
Sh 2-68	30.673	6.279	18 24 58.43	0 51 36.02	200										
A 43	36.062	17.62	17 53 32.28	10 37 24.21	40	-42 ± 11.5	5 ± 0.5	4276328581046447104	400	-19.06 ± 0.12	-56.06 ± 0.13	16.4	0.28		
NGC 6852	42.59	-14.528	20 0 39.21	1 43 40.92	14	-11 ± 5	40 ± 2	4488953930631143168	2187	-5.61 ± 0.11	1.03 ± 0.1	14.7	-0.28		
Sh 2-78	46.832	3.845	19 3 10.08	14 6 58.78	298	42 ± 1.7	43.1 ± 4.3	4237745794618477440	3099	-1.38 ± 0.27	-4.75 ± 0.2	17.9	-0.34		
A 72	59.795	-18.729	20 50 2.05	13 33 29.52	68	-59 ± 23	20 ± 2	4506484097383382272	629	-1.11 ± 0.21	-4.21 ± 0.22	17.6	-0.05		
NGC 6765	62.458	9.557	19 11 6.56	30 32 43.68	17	-64 ± 14.6	35 ± 3.5	1761341417799128320	1395	1.46 ± 0.11	-6.28 ± 0.09	16	-0.54		
NGC 7094	66.778	-28.202	21 36 52.97	12 47 19.1	50	-101 ± 30.8	38 ± 2	2039515046433996544	3476	-0.61 ± 0.25	-4.3 ± 0.34	17.5	-0.2		
Kr 61	70.524	11.007	19 21 38.94	38 18 57.22	48	-25.4 ± 2	67.6 ± 6.8	1770058865674512896	1548	3.61 ± 0.09	-10.6 ± 0.09	13.5	-0.45		
MWP 1	80.356	-10.409	21 17 8.28	34 12 27.42	336		30 ± 3	2052811676760671872	3306	-0.1 ± 0.29	-3.78 ± 0.26	18.3	-0.47		
Jacoby 1	85.366	52.349	15 21 46.56	52 22 3.87	330		30 ± 3	1855295171732158080	495	-5.47 ± 0.07	10.44 ± 0.08	13	-0.59		
K 1-16	94.025	27.428	18 21 52.11	64 21 53.41	57		22.5 ± 2.3	1595941441250636672	734	-3.96 ± 0.1	11.26 ± 0.14	15.6	-0.66		
Jn 1	104.208	-29.642	23 35 53.32	30 28 6.34	163	-67 ± 30	15 ± 1.5	2160562927224840576	1986	-3.27 ± 0.13	-3.05 ± 0.11	15	-0.63		
NGC 246	118.863	-74.709	0 47 3.34	-11 52 18.98	122	-46 ± 3.6	39.5 ± 4	185295171732158080	808	2.97 ± 0.13	-4.3 ± 0.09	16	-0.53		
NGC 650	130.934	-10.504	1 42 19.66	51 34 31.55	70	-19 ± 1.2	39 ± 3.9	2376592910265354368	506	-16.96 ± 0.21	-9 ± 0.13	11.8	-0.65		
IsWe 1	149.715	-3.398	3 49 5.91	50 0 14.9	363	-2 ± 0.5	12 ± 1.2	406328439057955968	2873	-0.25 ± 0.81	-4.16 ± 0.47	17.3	0.02		
JnEr 1	164.806	31.181	7 57 51.62	53 25 16.94	190	-84 ± 8.8	24 ± 2.4	250358801943821952	441	18.01 ± 0.17	-7.43 ± 0.13	16.5	-0.26		
A 21	205.139	14.241	7 29 2.71	13 14 48.59	316	29 ± 5.2	32 ± 3.2	936605992140011392	979	0.14 ± 0.15	-0.72 ± 0.12	17.1	-0.63		
Lo 3	258.068	-15.748	7 14 49.42	-46 57 39.21	47		15.6 ± 1.6	3163546505053645056	531	-2.72 ± 0.14	-8.6 ± 0.13	16	-0.59		
Lo 4	274.309	9.112	10 5 45.79	-44 21 33.52	20			5509004952576699904	1807	0.84 ± 0.2	4.46 ± 0.23	16.8	-0.04		
								5414927915911816704	3180	-6.15 ± 0.12	0.3 ± 0.13	16.6	-0.47		

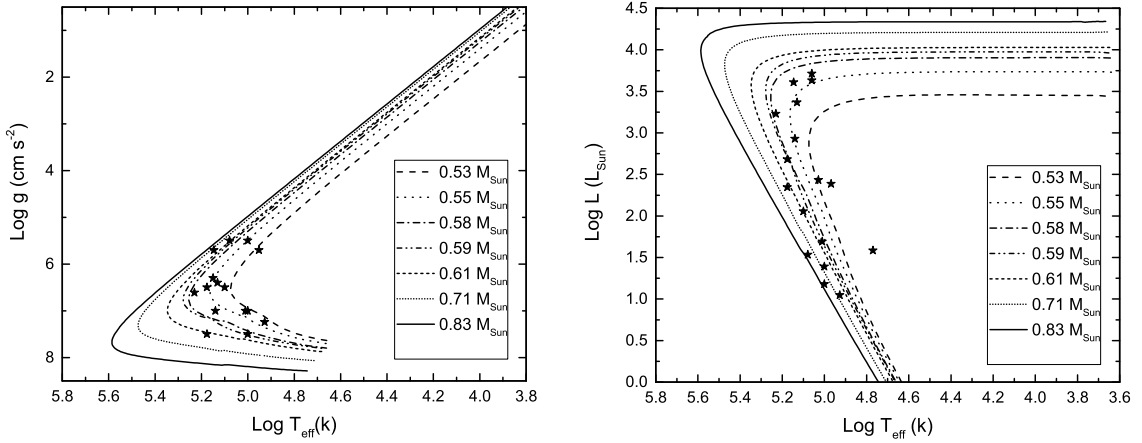


Fig. 1 Location of PG 1159 CSs on the H-R diagram. The hydrogen-burning evolutionary tracks overlaid on the diagram are taken from [Miller Bertolami \(2016\)](#) with initial metallicity of $Z = 0.001$. The *left* and *right* panels display the position of PG 1159 stars on $\log T_{\text{eff}} - \log g$ and $\log T_{\text{eff}} - \log L$ charts, respectively. The final mass of each model star is given on both charts. To clarify the figure, the evolutionary age isochrones of various stellar models and PNe names are omitted.

temperature and surface gravity were extracted from [Weidmann et al. \(2020\)](#) and [Werner & Herwig \(2006\)](#), whereas the luminosity was derived from the Gaia distance and CS visual magnitude, corrected for interstellar extinction, following [Frew \(2008\)](#). The PN extinction coefficients are gathered from [Frew et al. \(2016\)](#). Figure 1 shows the Hertzsprung-Russell (H-R) diagram of the CS sample in which the left and right panels depict the locations of the PG 1159 stars, that have available data, on the $\log T_{\text{eff}} - \log g$ and $\log T_{\text{eff}} - \log L$ charts, respectively. The H-burning post-AGB tracks with diverse masses and initial metallicity $Z = 0.001$ ([Miller Bertolami 2016](#)) are overlaid on both charts. These tracks describe the theoretical evolution of seven model stars with different

initial masses ($0.9, 1.0, 1.25, 1.75, 2.0, 2.5$ and $3 M_{\odot}$) from the onset of post-AGB phase until the end of WD cooling sequence phase. The final stellar masses of the diverse stellar models ($0.53, 0.55, 0.58, 0.59, 0.61, 0.71$ and $0.83 M_{\odot}$) are illustrated in the figure. Most PG 1159 stars reside close to the tracks with final stellar masses less than $0.59 M_{\odot}$. The average final mass of the PG 1159 stars is $0.58 \pm 0.08 M_{\odot}$, which is slightly smaller than the value ($0.62 M_{\odot}$) derived by [Werner & Herwig \(2006\)](#). From the age isochrones, we infer the evolutionary age (T_{ev}) of each star. The estimated final mass and evolutionary age of the PG 1159 stars are expressed in Table 2. The results show acceptable agreement between the evolutionary age of each PG 1159 star and its companion PN dynamical

Table 2 The physical parameters of the sample, where R , T_{dyn} , V_{LSR} and $|V_p|$ are the PN radius, dynamical age, line of sight velocity corrected for LSR and absolute peculiar velocity, respectively. T_{ev} and M_f are the evolutionary age and final mass of the CS, respectively.

PN designation	R (pc)	$T_{\text{dyn}} \times 10^3$ (yr)	$T_{\text{ev}} \times 10^3$ (yr)	M_f (M_{\odot})	V_{LSR} (km s^{-1})	$ V_p $ (km s^{-1})
Sh 2-68	0.39 ± 0.04	75.8 ± 11.0	104.0 ± 15.0	0.63 ± 0.11		
A 43	0.42 ± 0.07	10.4 ± 1.8	8.3 ± 1.7	0.57 ± 0.06	-27.08 ± 7.41	90 ± 11
NGC 6852	0.20 ± 0.09	4.6 ± 2.1		0.53 ± 0.00	4.13 ± 1.88	99 ± 56
Sh 2-78	0.91 ± 0.12	44.4 ± 7.3	37.3 ± 8.0	0.65 ± 0.09	56.35 ± 2.29	24 ± 2.4
A 72	0.46 ± 0.08		67.0 ± 13.0		-43.38 ± 17.03	87 ± 17
NGC 6765	0.29 ± 0.14	8.0 ± 4.0		0.53 ± 0.00	-49.35 ± 11.21	134 ± 36
NGC 7094	0.38 ± 0.05	9.7 ± 1.4	8.6 ± 1.5	0.53 ± 0.00	-86.23 ± 26.27	125 ± 26
Kr 61	0.77 ± 0.34	11.1 ± 5.0			-11.13 ± 0.88	73 ± 15
MWP 1	0.81 ± 0.08	26.3 ± 5.6	3.4 ± 0.8	0.58 ± 0.00		
Jacoby 1	1.17 ± 0.17	38.3 ± 10.0	5.8 ± 1.8	0.58 ± 0.06		
K 1-16	0.54 ± 0.08	23.7 ± 4.2	12.5 ± 2.0	0.53 ± 0.00		
Jn 1	0.64 ± 0.08	41.6 ± 6.7	10.6 ± 1.8	0.56 ± 0.04	-56.68 ± 25.38	76 ± 26
NGC 246	0.30 ± 0.03	7.4 ± 1.1	8.3 ± 2.1	0.59 ± 0.04	-38.82 ± 3.04	45 ± 3.1
NGC 650	0.97 ± 0.41	24.4 ± 11.0	9.9 ± 1.9	0.56 ± 0.04	-15.63 ± 0.98	3 ± 5
IsWe 1	0.77 ± 0.08	63.1 ± 22.0	53.4 ± 2.6	0.65 ± 0.17	-3.36 ± 1.12	12 ± 1.1
JnEr 1	0.90 ± 0.13	36.8 ± 7.0	44.5 ± 5.4	0.56 ± 0.04	-86.16 ± 8.99	87 ± 9
A 21	0.81 ± 0.09	24.8 ± 2.6	22.5 ± 7.0	0.58 ± 0.06	17.85 ± 3.22	24 ± 3.2
Lo 3	0.41 ± 0.10	25.8 ± 6.6	10.0 ± 2.2	0.53 ± 0.00		
Lo 4	0.31 ± 0.08		1.5 ± 0.5	0.74 ± 0.04	23.79 ± 14.42	54 ± 14

Table 3 The Effective Temperature, Surface Gravity and Luminosity of the PG 1159 CSs

PN designation	$\log T_{\text{eff}}$ (K)	$\log g$ (cm s^{-2})	$\log L$ (L_{\odot})
Sh 2-68	4.93	7.24	1.05
A 43	5.00	5.50	3.29
NGC 6852	4.77		1.59
Sh 2-78	5.00	7.50	1.39
A 72	5.03		2.43
NGC 6765	4.97		2.39
NGC 7094	4.95	5.70	3.40
Kr 61			
MWP 1	5.23	6.61	3.23
Jacoby 1	5.18	7.50	2.34
K 1-16	5.13	6.40	3.37
Jn 1	5.18	6.50	2.68
NGC 246	5.15	5.70	3.61
NGC 650	5.14	7.00	2.93
IsWe 1	5.00	7.00	1.18
JnEr 1	5.01	7.00	1.69
A 21	5.10	6.50	2.05
Lo 3	5.15	6.30	
Lo 4	5.08	5.50	1.53

age (Table 2). The derived mean evolutionary age of the PG 1159 stars, $25.5 \pm 5.3 \times 10^3$ yr, is slightly lower than the calculated mean nebular dynamical age ($28.0 \pm 6.4 \times 10^3$ yr).

4 KINEMATICAL CHARACTERISTICS OF THE SAMPLE

4.1 Toomre Diagram

The Toomre diagram has been introduced by [Bensby et al. \(2003\)](#) and [Bensby et al. \(2010\)](#) to carefully investigate the Galactic population of F and G dwarfs. To construct this diagram, we derived the space velocity components (U , V and W) and their uncertainties following the procedure suggested by [Johnson & Soderblom \(1987\)](#). We ignored

the errors associated with the equatorial and galactic coordinates, which have an insignificant effect on the final results. The uncertainties in the U , V and W components were estimated by propagating errors in the distance, radial velocity and proper motion. U and V denote the Galactic center and Galactic rotation directions, respectively, whereas W indicates the direction perpendicular to the Galactic disk. The velocity components were corrected for the local standard of rest (LSR) assuming that the solar peculiar motion $(U_{\odot}, V_{\odot}, W_{\odot}) = (9.0, 11.0, 6.0) \text{ km s}^{-1}$. The space velocity component V , presented in Table 4, is corrected further for the rotational solar velocity $V(R_{\odot}) = 220 \text{ km s}^{-1}$. To locate the sample objects on the Toomre diagram, we calculate their total space velocities V_S ($\sqrt{U_{\text{LSR}}^2 + V_{\text{LSR}}^2 + W_{\text{LSR}}^2}$).

In the Toomre diagram, stars with $V_S \leq 50 \text{ km s}^{-1}$ are located in the Galactic thin disk and those with $200 \geq V_S \geq 70 \text{ km s}^{-1}$ reside in the Galactic thick disk, while stars with $V_S > 200 \text{ km s}^{-1}$ settle in the Galactic halo. Objects with $70 \geq V_S \geq 50 \text{ km s}^{-1}$ have similar likelihood to exist either in the Galactic thin or thick disk. Figure 2 affirms that A 21 and IsWe 1 are associated with the Galactic thin disk, while NGC 246, NGC 6765, NGC 6852, JnEr 1, NGC 7094, A 43 and Lo 4 are associated with the Galactic thick disk. The nebulae NGC 650, Kr 61, A 72, Sh 2-78 and Jn 1 have equal probability of belonging to either the Galactic thin or thick disk. In addition to the space velocity components of the studied objects, we present, in Table 4, their space coordinates X (towards the Galactic anti-center), Y and Z (towards the Galactic North Pole). We adopt here the solar space coordinates $X_{\odot} = 7.6 \text{ kpc}$, $Y_{\odot} = 0.0$ and $Z_{\odot} = 0.0$.

Table 4 Space Coordinates and Velocity Components of the Sample

PN designation	X (pc)	Y (pc)	Z (pc)	U (km s ⁻¹)	V (km s ⁻¹)	W (km s ⁻¹)	V_s (km s ⁻¹)
Sh 2–68	7258	203	44				
A 43	5915	1227	662	-27.0 ± 7.0	179.0 ± 28.0	49.0 ± 10.0	69.4 ± 27.0
NGC 6852	5391	2030	777	47.2 ± 25.3	163.4 ± 63.2	-5.5 ± 3.3	73.9 ± 61.0
Sh 2–78	7171	458	42	48.0 ± 1.9	247.0 ± 16.9	7.0 ± 50.0	55.5 ± 72.0
A 72	6935	1142	448	1.3 ± 1.7	154.5 ± 41.5	-4.3 ± 3.2	65.7 ± 41.0
NGC 6765	6015	3039	577	43.0 ± 41.0	141.0 ± 32.0	-25.0 ± 9.0	93.4 ± 33.0
NGC 7094	7062	1254	731	-0.2 ± 0.3	96.4 ± 18.9	-7.6 ± 8.1	123.8 ± 19.0
Kr 61	6518	3059	631	54.0 ± 27.9	188.6 ± 32.0	-22.1 ± 8.6	66.3 ± 32.0
MWP 1	7518	480	90				
Jacoby 1	7564	447	581				
K 1–16	7724	1758	915				
Jn 1	7772	681	400	13.0 ± 29.0	166.0 ± 70.0	40.0 ± 18.0	68.4 ± 68.0
NGC 246	7664	117	488	62.0 ± 3.0	219.0 ± 32.0	46.0 ± 4.0	77.2 ± 30.0
NGC 650	9451	2134	524	23.0 ± 15.0	198.0 ± 65.0	-45.0 ± 20.0	55.1 ± 63.0
IsWe 1	7980	222	26	-9.0 ± 0.4	191.0 ± 7.2	18.0 ± 0.8	35.3 ± 7.2
JnEr 1	8408	220	507	79.0 ± 8.0	203.0 ± 19.0	-36.0 ± 4.0	88.5 ± 18.0
A 21	8066	-218	131	-11.6 ± 2.5	197.0 ± 15.7	-0.7 ± 0.1	25.8 ± 16.0
Lo 3	7960	-1701	490				
Lo 4	7364	-3131	504	-64.0 ± 16.1	179.0 ± 77.1	-38.0 ± 10.8	85.0 ± 72.0

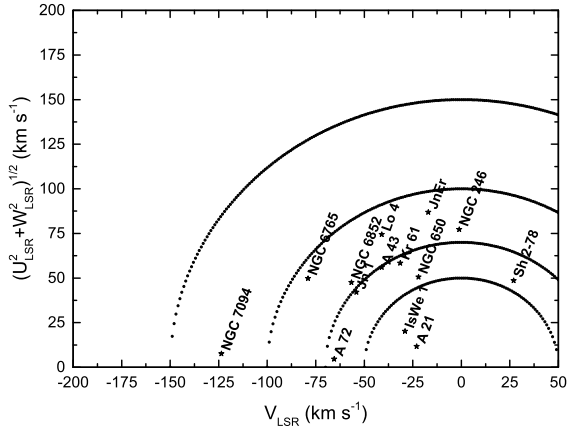


Fig. 2 Toomre diagram of our sample. The space velocity components U , V and W are corrected for the LSR. *Dotted semi-circular lines* demonstrate constant total space velocity values: 50, 70, 100 and 150 km s⁻¹. The error bars for each PN were removed to clarify the figure.

4.2 Peculiar Velocity

Peculiar velocity (V_p) expresses the difference between the line of sight velocity corrected for LSR and the velocity derived from the Galactic rotation curve, assuming the object has a circular orbit (Quiroza et al. 2007). Maciel & Dutra (1992) proposed the concept of peculiar velocity to distinguish between the different types of Peimbert classification (Peimbert 1978). According to this classification, Quiroza et al. (2007) consider all PNe moving with $|V_p| \geq 60$ km s⁻¹ as high velocity nebulae of Peimbert type III while those moving with $|V_p| < 60$ km s⁻¹ as low velocity nebulae of Peimbert types I and II. Although Peimbert types are mainly based on the chemical composition of the PNe, they show further variation in their kinematical properties. Type I and II PNe are members of Galactic population I that live in

the Galactic thin disk, while type III PNe are members of Galactic population II that live in the Galactic thick disk. In general, PNe arise from a wide stellar mass domain ranging from $0.8 M_\odot$ to $8.0 M_\odot$. Peimbert type III nebulae mostly originate from the lower progenitor mass stars compared to types I and II. As a result of scarce information regarding the observed chemical abundances of nearly all PNe in the sample, it is difficult to get their Peimbert types. Based on the modest abundances of a few chemical elements in some objects and using the Bayes theorem, Quiroza et al. (2007) were able to predict the classifications of Peimbert type III for NGC 6765 and type IIa for Jn 1, NGC 246 and NGC 650.

The absolute peculiar velocities are calculated following Quiroza et al. (2007) and the results are presented in Table 2. We found eight objects out of 14 possessing $|V_p| \geq 60$ km s⁻¹ and two objects possessing $|V_p| \geq 45$ km s⁻¹. This refers to a moderate tendency for the nebular sample to be of Peimbert type III and, hence, they mostly belong to the Galactic thick disk and originated from low mass stars. The derived peculiar velocities agree with the results deduced from the Toomre diagram (Sect. 4.1) where the objects with small peculiar velocities, e.g., IsWe 1 ($|V_p| = 12 \pm 1.1$ km s⁻¹) and A 21 ($|V_p| = 24 \pm 3.2$ km s⁻¹) occupy the Galactic thin disk, whereas objects with high velocities, e.g., NGC 6765 ($|V_p| = 134 \pm 36$ km s⁻¹) and NGC 7094 ($|V_p| = 125 \pm 26$ km s⁻¹) occupy the Galactic thick disk.

It is noticeable that although NGC 650 has insignificant peculiar velocity, it has high galactic latitude and vertical height. Further, its measured total space velocity indicates that the location of this object is in the area of overlap between the thin and thick Galactic disk ($70 \geq V_S \geq 50$ km s⁻¹). The former results promoted the likelihood membership of NGC 650 to the Galactic thick

disk instead of the thin disk. Taking into consideration the galactic heights and peculiar velocities, we found that Kr 61, A 72 and Jn 1 (that also lie in the overlapping area between the Galactic thin and thick disk on the Toomre diagram) have much tendency to belong to the Galactic thick disk, whereas Sh 2-78 to the Galactic thin disk.

5 ARE A 21, IeWe 1, Sh 2-78 AND NGC 650 REALLY ASSOCIATED WITH PG 1159 CSs?

The nebulae A 21, IeWe 1, Sh 2-78 and NGC 650 hold faint CSs with visual magnitudes 17.94 ± 0.03 (Pena et al. 1997), 16.56 ± 0.10 (Ishida & Weinberger 1987), 17.78 ± 0.03 (Cappellaro et al. 1990) and 17.70 ± 0.20 (Napiwotzki 1993), respectively. These four CSs are classified as PG 1159 type by Napiwotzki (1992) and Napiwotzki (1993) using low-resolution spectra. Pena et al. (1997) noticed the presence of shallow and wide hydrogen and helium absorption lines in the optical spectrum of the A 21 CS indicating a hot hydrogen-rich WD of DAO spectral type. This result disagrees with the prior classification of this star as a PG 1159 spectral type (Napiwotzki 1993). Unfortunately, no recent medium or high dispersion spectra are available for the other three stars to confirm their early PG 1159 classification.

6 CONCLUSIONS

We have conducted an analysis for the available PNe that host CSs of spectral type PG 1159. The kinematical and physical characteristics of PNe-PG 1159 objects were discussed in detail. The leading results clearly point out that the majority of these nebulae belong to the Galactic thick disk population. Furthermore, they are evolved PNe of Peimbert type III that originated from low mass progenitor stars. The mean dynamical age of the nebular sample exhibits good agreement with the mean evolutionary age of their PG 1159 CSs, and both are about three times the standard value. A further argument confirming the aging of these nebulae is their mean large size, which is about six times the common nebular size. Finally, it is worth noting that the sample utilized in this analysis is statistically small to set up solid conclusions.

Acknowledgements The authors would like to thank the anonymous referee for his/her valuable comments that enhanced the paper. Further, we appreciate the useful remarks of Dr. Awad, Z. and Dr. Snaid, S., which helped us improve the reading of the paper. This work has made use of data from the European Space Agency (ESA) mission Gaia, processed by the Gaia Data Processing and Analysis Consortium (DPAC). This research has made use of the SIMBAD database, operated at CDS, Strasbourg, France.

References

- Acker, A., Fresneau, A., Pottasch, S. R., & Jasniewicz, G. 1998, *A&A*, 337, 253
- Acker, A., Marcout, J., Ochsenbein, F., et al. 1992, *The Strasbourg-ESO Catalogue of Galactic Planetary Nebulae. Parts I, II.* (European Southern Observatory, Garching (Germany), 1992, 1047, ISBN 3-923524-41-2)
- Ali, A., Ismail, H. A., & Alsolami, Z. 2015, *Ap&SS*, 357, 21
- Bailer-Jones, C. A. L., Rybizki, J., Fouesneau, M., et al. 2018, *AJ*, 156, 58
- Bensby, T., Feltzing, S., & Lundström, I. 2003, *A&A*, 410, 527
- Bensby, T., Feltzing, S., Johnson, J. A., et al. 2010, in *IAU Symposium*, 265, *Chemical Abundances in the Universe: Connecting First Stars to Planets*, eds. K. Cunha, M. Spite, & B. Barbuy, 346
- Brown, A., Vallenari, A., Prusti, T., & et al. 2018, *A&A*, 616, A1
- Cappellaro, E., Turatto, M., Salvadori, L., & Sabbadin, F. 1990, *A&AS*, 86, 503
- Carollo, D., Beers, T. C., Chiba, M., et al. 2010, *ApJ*, 712, 692
- Frew, D. J. 2008, *Planetary Nebulae in the Solar Neighbourhood: Statistics, Distance Scale and Luminosity Function*, PhD thesis, Macquarie University, NSW 2109, Australia
- Frew, D. J., Parker, Q. A., & Bojičić, I. S. 2016, *MNRAS*, 455, 1459
- Harris, H. C., Dahn, C. C., Canzian, B., et al. 2007, *AJ*, 133, 631
- Ishida, K., & Weinberger, R. 1987, *A&A*, 178, 227
- Johnson, D. R. H., & Soderblom, D. R. 1987, *AJ*, 93, 864
- Löbbling, L., Rauch, T., Miller Bertolami, M. M., et al. 2019, *MNRAS*, 489, 1054
- Maciel, W. J., & Dutra, C. M. 1992, *A&A*, 262, 271
- Mendez, R. H. 1991, in *NATO Advanced Science Institutes (ASI) Series C*, 341, *NATO Advanced Science Institutes (ASI) Series C*, eds. L. Crivellari, I. Hubeny, & D. G. Hummer, 331
- Miller Bertolami, M. M. 2016, *A&A*, 588, A25
- Napiwotzki, R. 1992, *Analysis of Central Stars of Old Planetary Nebulae: Problems with the Balmer Lines*, eds. U. Heber & C. S. Jeffery, 401, 310
- Napiwotzki, R. 1993, *Acta Astronomica*, 43, 343
- Napiwotzki, R., & Schoenberner, D. 1991, *A&A*, 249, L16
- Peimbert, M. 1978, in *IAU Symposium*, 76, *Planetary Nebulae*, ed. Y. Terzian, 215
- Pena, M., Ruiz, M. T., Bergeron, P., et al. 1997, *A&A*, 317, 911
- Pottasch, S. R. 1983, in *Planetary Nebulae*, ed. L. H. Aller, 103, 391
- Pottasch, S. R., & Acker, A. 1998, *A&A*, 329, L5
- Quireza, C., Rocha-Pinto, H. J., & Maciel, W. J. 2007, *A&A*, 475, 217
- Weidmann, W. A., & Gamen, R. 2011, *A&A*, 526, A6
- Weidmann, W. A., Mari, M. B., Schmidt, E. O., et al. 2020, *A&A*, 640, A10
- Werner, K., & Herwig, F. 2006, *PASP*, 118, 183